Vol 17 No 2, February 2008
1674-1056/2008/17(02)/0649-06

Chinese Physics B

© 2008 Chin. Phys. Soc.
and IOP Publishing Ltd

Effect of an axial magnetic field on a DC argon arc*

Li Lin-Cun(黎林村) and Xia Wei-Dong (夏维东)†

Department of Thermal Science & Energy Engineering, University of Science & Technology of China, Hefei 230027, *China*

(Received 21 March 2007; revised manuscript received 19 April 2007)

In this paper a commercial CFD (computational fluid dynamics) code FLUENT has been used and modified for the axisymmetric swirl and time-dependent simulation of an atmospheric pressure argon arc in an external axial magnetic field (AMF). The computational domain includes the arc itself and the anodic region. Numerical results demonstrate that the AMF substantially increases the tangential component of the plasma velocity. The resulting centrifugal force for the plasma rotation impels it to travel to the arc mantel and as a result, a low-pressure region appears at the arc core. With the AMF, the arc presents a hollow bell shape and correspondingly, the maximal values of the temperature, pressure and current density on the anode surface are departing from the arc centreline.

Keywords: arc modeling, axial magnetic field, FLUENT
PACC: 5230, 5265, 5280

1. Introduction

Transferred arcs at atmospheric pressure have found application in many different manufacturing processes including melting and refining of materials and wasters, metal cutting and welding.[1−9] The behaviour of the arc can be easily affected and changed by an axial magnetic field (AMF) parallel to its centreline.[8,9] The AMF will produce a Lorentz force and induce the rotation of plasmas, and the resulting centrifugal force will significantly influence the fluid flow and heat transfer inside the arc.

Even though many excellent simulation papers have been published about the transferred arc in the recent past,[10−15] a time-dependent modelling of an AMF arc including the anodic region in the computational domain has not been developed so far, to the authors' knowledge. The aim of this work is to evaluate the transient effect of an imposed AMF on the behaviour of the arc by means of an axisymmetric swirl time-dependent numerical model, using a customized version of the computational fluid dynamics (CFD) commercial code FLUENT. In this study, unsteady flow and heat transfer equations are solved together with the equations of the electric potential and the magnetic vector potential, over a computational domain that includes the arc itself and a copper anode.

2. Mathematical model

The arc configuration is schematically represented in Fig.1. A DC argon arc burns between a pin cathode and a copper plate anode, the diameter of the cathode is 3 mm and its tip angle is 60°. The cathode–anode

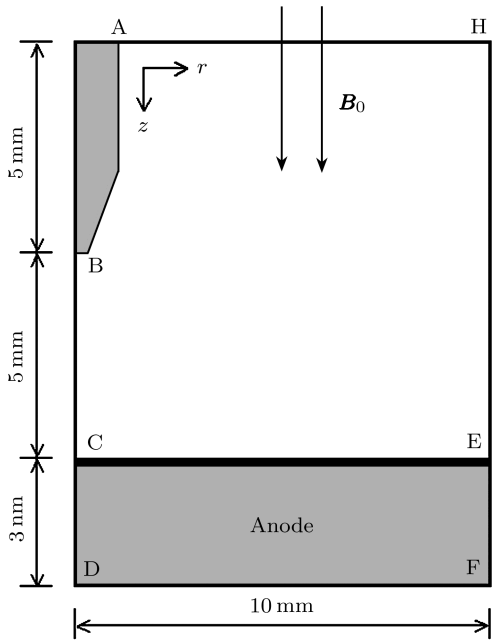


Fig.1. Geometry and coordinate system for an AMF arc.

*Project supported by the National Natural Science Foundation of China (Grant Nos 10375065 and 10675122).
†Corresponding author. E-mail: xiawd@ustc.edu.cn

distance is chosen equal to 5 mm and the anode thickness is taken to be 3 mm. A uniform longitudinal magnetic field is imposed in the entire plasma domain. The numerical model of this arc relies on the following main assumptions:

2.1. Assumptions

The plasma flow is laminar.

The arc is in local thermodynamic equilibrium (LTE), which is taken to mean that the electron and heavy particle temperatures are not significantly different.

The plasma is assumed to be optically thin so that radiation may be accounted for using an optically thin radiation loss per unit volume.

Pressure variation in the flow-field is assumed to be insignificant so that compressibility effects are neglected. The thermodynamic and transport properties of argon plasma just are functions of the local temperature.

The heating effects of viscous dissipation, and buoyancy force due to gravity are neglected.

The effects of anode melting and vaporization are neglected.

The induced current is small in comparison with the arc current and it is therefore neglected.

2.2. Governing equations

Based on the foregoing assumptions, the axisymmetric swirl unsteady governing equations for the AMF arc can be written as follows:

2.2.1. Mass

$$\frac{\partial \rho}{\partial t} + \nabla \cdot (\rho \boldsymbol{V}) = 0. \tag{1}$$

2.2.2. Momentum

$$\begin{aligned} &\frac{\partial (\rho \boldsymbol{V})}{\partial t} + \nabla \cdot (\rho \boldsymbol{V}\boldsymbol{V}) \\ &= -\nabla p + \nabla \cdot \left[\mu \cdot \left(\nabla \boldsymbol{V} + \nabla \boldsymbol{V}^{\mathrm{T}}\right)\right] \\ &\quad + \boldsymbol{J} \times (\boldsymbol{B} + \boldsymbol{B}_0)\,. \end{aligned} \tag{2}$$

2.2.3. Energy

$$\begin{aligned} &\frac{\partial (\rho h)}{\partial t} + \nabla \cdot (\rho \boldsymbol{V} h) \\ &= \nabla \cdot \left(\frac{k}{c_{\mathrm{p}}} \cdot \nabla h\right) \\ &\quad + \boldsymbol{J} \cdot \boldsymbol{E} + \frac{5}{2}\frac{k_{\mathrm{B}}}{e}\left(\frac{\boldsymbol{J}}{c_{\mathrm{p}}} \cdot \nabla h\right) - S_{\mathrm{R}}. \end{aligned} \tag{3}$$

2.2.4. Electric potential

$$\nabla \cdot (\sigma \nabla \phi) = 0, \quad \boldsymbol{J} = -\sigma \nabla \phi, \quad \boldsymbol{E} = -\nabla \phi. \tag{4}$$

2.2.5. Magnetic field

$$\nabla^2 \boldsymbol{A} = -\mu_0 \boldsymbol{J}, \quad \boldsymbol{B} = \nabla \times \boldsymbol{A}. \tag{5}$$

In these above equations, $\boldsymbol{V}$ is the plasma velocity and p, h, ϕ denote the pressure, plasma enthalpy, and electric potential respectively. $\boldsymbol{J}$ is the current density, $\boldsymbol{B}, \boldsymbol{B}_0$ are the self-induced and external magnetic fields respectively. $\boldsymbol{E}$ denotes the electrical field and $\boldsymbol{A}$ is the magnetic vector potential. $\rho, \mu, k, c_{\mathrm{p}}, \sigma, S_{\mathrm{R}}, \mu_0, k_{\mathrm{B}}, e$ are orderly the plasma density, viscosity, thermal conductivity, specific heat, electric conductivity, volumetric radiation power, permeability of free space, Boltzmann's constant and elementary electric charge.

In the anode region, the energy and electric-potential equations are solved. In the energy equation the convective terms are neglected and the only source term considered is the Joule heating.

The user-defined scalar (UDS) approach has been adopted for the treatment of the electromagnetic field, and user-defined functions (UDF) have been written to implement the extra source terms and transport coefficients appearing in the transport equations.

The governing equations are solved on a structured computational grid made up of quads. The approximate number of cells making up the grid is 3.0×10^3, while the time step adopted throughout the calculations is $\Delta t = 10^{-5}$ s. The grid was concentrated near the electrodes to capture the steep temperature gradient in the arc column.

2.3. Boundary conditions

The interaction between the plasma and the cathode is not modelled in this study. The boundary conditions used are indexed as following:

At the inflow surface AH, the gas flow is assumed to be perpendicular to the boundary and its velocity, temperature are set to be 5 m/s, 1000 K respectively.

The FLUNET-implemented 'pressure-outlet' is selected as the boundary condition at the outflow surface FH.

Both AH and FH have zero current flux.

The traditional no-slip condition is imposed on the electrodes. The temperature of the cathode surface AB is specified to be 3500 K and as a potential boundary condition at the cathode tip, we use the current density distribution expressed by numerous authors:[11,13]

$$j(r) = J_{\max} \exp(-br). \tag{6}$$

In this study, $J_{\max}$ is chosen to be $1.2 \times 10^8 \mathrm{A/m^2}$ and the constant number b is adjusted to conserve the current intensity.

Physically, the plasma is not in LTE at the anode sheath, the heavy particle temperature is close to that of the anode material while the electron temperature is much higher. To simplify the modelling, we use the electrical conductivity of the anode material but the viscosity, the thermal conductivity and the specific heat of the plasma gas are in this zone.[13]

In order to maintain energy and current conservations between the plasma and the anode, the following equations are used at the interface CF.[14]

$$\left[-\sigma\left(\frac{\partial\phi}{\partial z}\right)\right]_{\text{anode}} = \left[-\sigma\left(\frac{\partial\phi}{\partial z}\right)\right]_{\text{plasma}}, \tag{7}$$

$$\left[-k\left(\frac{\partial T}{\partial z}\right)\right]_{\text{anode}} = \left[-k\left(\frac{\partial T}{\partial z}\right)\right]_{\text{plasma}} + j_z \cdot \left[\frac{5}{2}\cdot\frac{k_{\mathrm{B}}}{e}\cdot(T_{\text{plasma}} - T_{\text{anode}}) + (\phi_{\mathrm{a}} + \phi_{\mathrm{s}})\right], \tag{8}$$

where, ϕ_{a} and ϕ_{s} are the anode voltage fall and the anode work function respectively. For our configurations, the anode work function is 4.65 V and the anode voltage fall is neglected in equation (8) as suggested in Ref.[15]. The radiation between the arc and anode is neglected here as the fact that in the arc attachment zone, the radiation is much smaller than the heat flux due to the charge motion and the conduction.[15]

The underside of the anode DE, is taken to be a zero equipotential surface and its temperature is imposed to be 1000 K.

3. Results and discussion

The governing equations are solved with 200A arc current and 200 Gauss AMF strength. The results are reported in the form of snapshots taken at different times and the AMF is instantaneously turned on after the time $t = 0$.

Figures 2, 3 and 4 present the plasma temperature, velocity and pressure contours respectively. The effect of the AMF on the arc characteristics can be clearly found out from these comparative figures.

At the starting time $t = 0$ ms, i.e. when the AMF is absent, the arc is burning between the electrodes. A strong cathode jet impinges on the anode and forms the typical bell shape of the arc. Inside the arc, the highest plasma temperature, predicted to occur on the arc axis near the cathode tip, is about 21000 K, and as the arc spreads, the temperature drops to the value below 15000 K close to the anode sheath. The high temperature plasma is restricted around the arc axis mainly pinched by the arc self-electromagnetic force.

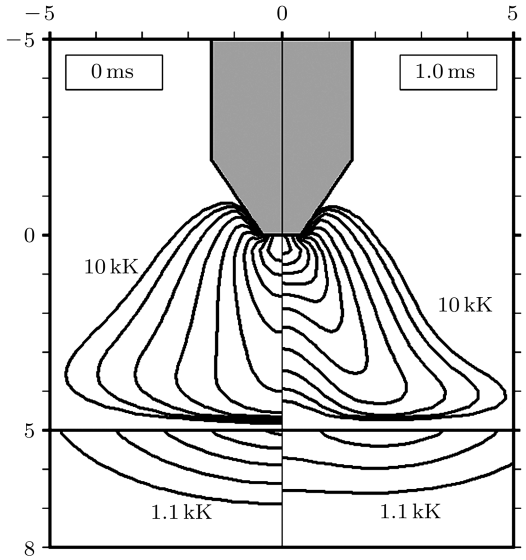


Fig.2. Temperature distributions inside the arc at $t = 0$ ms and $t = 1$ ms. (The intervals of the contour inside the arc are 1000 K, while they are 50 K in anode region).

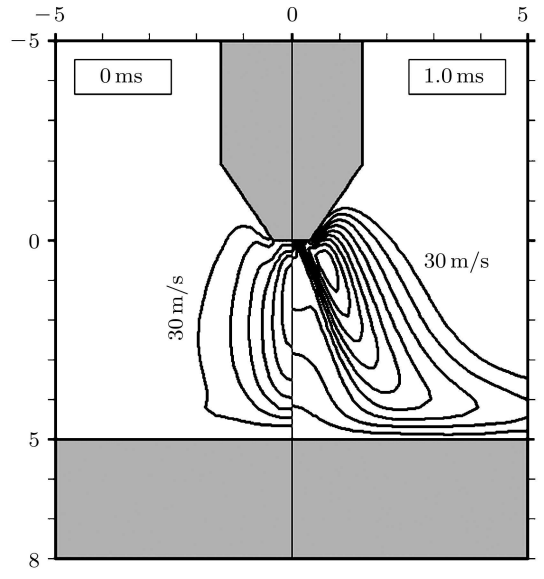


Fig.3. Velocity distributions inside the arc at $t = 0$ ms and $t = 1$ ms. (The intervals of the contour are 30 m/s)

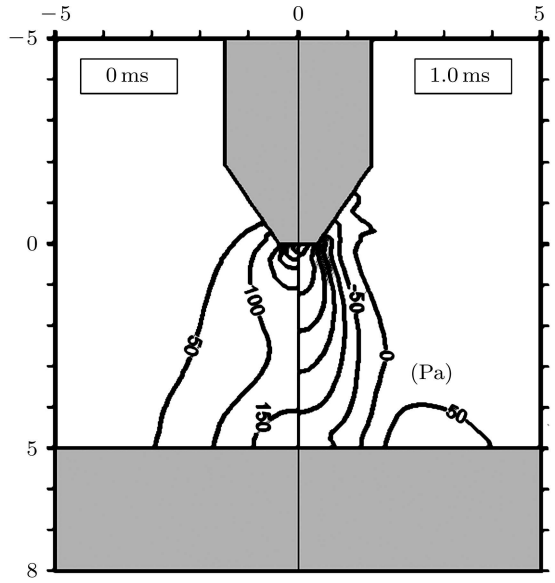


Fig.4. Pressure distributions inside the arc at $t = 0$ ms and $t = 1$ ms. (The intervals of the contour are 50 Pa).

The plasma velocity increases rapidly near the cathode tip due to the strong pressure gradient, a 145 m/s maximal velocity appears at the point $(z, r) = (1.4, 0)$ on the axis (the coordinate origin is located at the cathode tip), this means that most of the plasma flow through the arc core. The plasma stagnates in front of the anode, resulting in the velocity dropping sharply and the overpressure increasing there.

At the time $t = 1$ ms, i.e. while the AMF has been imposed. Although the highest plasma temperature keeps 21000 K and also occurs near the cathode tip, the high temperature plasma inside the arc is significantly retracted axially, especially where around the axis and expanded radially, the arc presents a hollow bell shape. The maximal plasma velocity magnitude increases to 207 m/s, which appears on the point $(z, r) = (0.6, 0.7)$ at the arc mantel, this means that most of the plasmas have flowed by there. The evolvement of the velocity components at this point is shown in Fig.5, we can see that the tangential and radial components of the plasma velocity, i.e. w and v respectively, have been substantially increased by the AMF. During $\Delta t = 1$ ms, w is increased from 0 to 172 m/s and v is increased from −17.8 to 23.5 m/s (the minus symbol just denotes the direction of the plasma flow and means the plasma flowing to the arc core here). The remoteness of the plasma at the arc core results in a low-pressure region there, the lowest pressure is equal to −350 Pa occurring on the cathode tip.

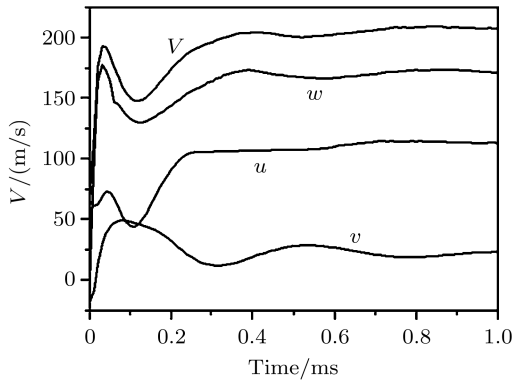


Fig.5. The evolution of the velocity components at the point $(z, r) = (0.6, 0.7)$.

In Fig.6, the distributions of the temperature, pressure and the current density on the interface CF are shown. Without the AMF, these distributions are quasi-normal, and the maximum values of these parameters are at arc centreline $r = 0$ mm. The presence of the AMF results in these maximum values appeared at $r = 2.3$ mm in accordance with the hollow arc shape. Compared to the non-AMF arc, the maximal current density of the AMF arc on CF has been decreased from 6.57 A/mm^2 to 3.45 A/mm^2. This is resulted from the AMF arc expanding radially and its conductive area on the interface increasing correspondingly. In accordance with the current density decrease (meaning the Joule heating weakening), the maximal temperature of the AMF arc decreases from 1316 K to 1223 K and the maximal pressure decreases from 182 Pa to 88 Pa at the interface.

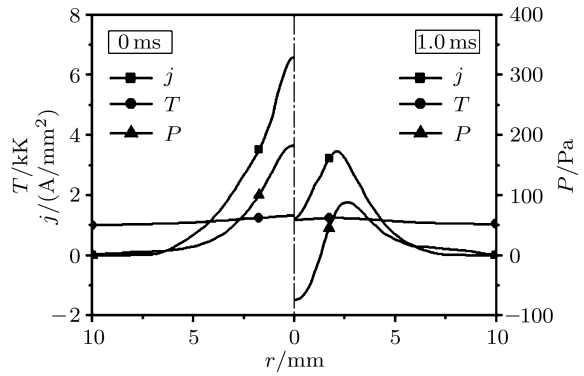


Fig.6. The distributions of the temperature, current density and pressure on the interface CF at $t = 0$ ms and $t = 1$ ms.

The evolution of the current density, temperature, axial velocity, and pressure at the point $(z, r) = (4, 0)$ in the arc area is shown in Fig.7. From the starting time to 0.35 ms, the current density and temperature keep on decreasing. Concretely, the current density is

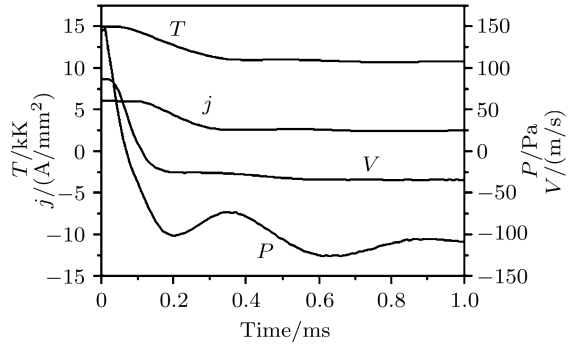


Fig.7. The evolution of the current density, temperature, velocity and pressure at the point $(z, r) = (4, 0)$.

descending from 6 A/mm^2 to 2.5 A/mm^2, and the temperature is descending about 4000 K, i.e. from 15000 K to 11000 K. After 0.35 ms, these two variables reach a steady state. During this time, although the value of axial velocity also trends to decrease monotonically, from 87 m/s to –30 m/s, the alterant symbol of the velocity value tells us that the plasma flow at the centreline should progress a great alteration: from impinging the anode surface to impinging the cathode tip. The evolvement of the pressure is undulant until the time $t = 0.9$ ms when it reaches a steady state. From the starting time, the pressure decreases sharply and reaches its first trough at $t = 0.2$ ms. Thereafter, it increases gently and achieves a small crest. The pressure reaches its second trough at $t = 0.6$ ms and subsequently increases again. Such an evolvement of the pressure is difficult to interpret, we propose that the gas flow plays an important role about evolvement of the pressure. The development of low-pressure region comes of the gas flow decreasing there.

Theoretically, inside the AMF arc, the plasmas are dominantly driven by the Lorentz force. It can be given by

$$\boldsymbol{F} = \boldsymbol{J} \times (\boldsymbol{B} + \boldsymbol{B}_0)\,. \tag{9}$$

The above equation indicates that in the plasma, which has radial velocity component, the swirl will be induced by the AMF and therefore its tangential velocity component should be substantially increased. The centrifugal force, resulting from the rotation, will impel the plasma to move to the arc mantel and thus increase its radial velocity component, so the movement of the plasma should present a spiral trace. With the plasma travelling to the arc mantel, the density of plasma at the arc core decreases and the arc presents the hollow bell shape.

4. Conclusion

In this paper, we have examined the electromagnetic fluid dynamics occurring in a DC argon arc subjected to an external AMF. An axisymmetric swirl time-dependent computer code has been developed on the base of a commercial CFD code FLUENT to predict the effect of the AMF on the arc characteristics. The modeling results, which are presented in the form of temperature, velocity, and pressure contours, show that the AMF arc is significantly retracted axially and expanded radially, most of the plasmas flow by the arc mantel and a low-pressure region is induced at the arc core, the AMF arc presents a hollow bell shape. These results clearly give an insight into the physical processes encountered in an AMF transferred arc situation.

References

[1] Fauchais P and Vardelle A 1997 *IEEE Trans. Plasma Sci.* **25** 1258

[2] Pfender E 1999 *Plasma Chem. Plasma Process.* **19** 1

[3] Zhang T, Hou J D, Tang B Y, Kwok T K, Zeng Z M, Brown I G and Chu P K 2000 *Chin. Phys.* **9** 279

[4] Karasik M and Zweben S L 2000 *Phys. Plasmas* **7** 4326

[5] Sun J S and Wu C S 2001 *Acta Phys. Sin.* **50** 209 (in Chinese)

[6] Sun J S, Wu C S and Zhang Y M 2002 *Acta Phys. Sin.* **51** 286 (in Chinese)

[7] Kogelschatz U 2004 *Plasma Phys. Control. Fusion* **46** 63

[8] Luo J, Jia C S, Wang Y S, Xue J and Wu Y X 2001 *Acta Metal. Sin.* **37** 212 (in Chinese)

[9] Luo J, Jia C S, Wang Y S, Xue J and Wu Y X 2001 *Acta Metal. Sin.* **37** 217 (in Chinese)

[10] Hsu K C, Etemadi K and Pfender E 1986 *J. Appl. Phys.* **54** 1293

[11] Freton P, Gonzalez J J and Gleizes A 2000 *J. Phys. D: Appl. Phys.* **33** 2442

[12] Marco A R, Gerardo T and John M 2003 *Modelling Simul. Mater. Sci. Eng.* **11** 675

[13] Lago F, Gonzalez J J, Freton P and Gleizes A 2004 *J. Phys. D: Appl. Phys.* **37** 883

[14] Franceries X, Lago F, Gonzalez J J, Freton P and Masquere M 2005 *IEEE Trans. Plasma Sci.* **33** 432

[15] Bini R, Monno M and Boulos M I 2006 *J. Phys. D: Appl. Phys.* **39** 3253